ACS APPLIED MATERIALS & INTERFACES

Research Article

www.acsami.org

Microporous Organic Polymers with Ketal Linkages: Synthesis, Characterization, and Gas Sorption Properties

Ying Han,[†] Li-Min Zhang,[†,‡] Yan-Chao Zhao,[‡] Tao Wang,[‡] and Bao-Hang Han*[,‡]

[†]College of Chemistry & Chemical Engineering, Yangzhou University, Yangzhou 225002, China

[‡]National Center for Nanoscience and Technology, Beijing 100190, China

Supporting Information

ABSTRACT: A series of microporous organic polymers with ketal linkages were synthesized based on the condensation of aromatic acetyl monomers with pentaerythritol. Fourier transform infrared and solid-state cross-polarization/magic-angle-spinning ^{13}C NMR spectroscopy were utilized to confirm the ketal linkages of the resulting polymers. The morphology can be observed from scanning electron microscopy and transmission electron microscopy images. The materials possess Brunauer–Emmet–Teller specific surface area values ranging from 520 to 950 $m^2\ g^{-1}$, and the highest hydrogen sorption capacity is up to 1.96 wt % (77 K and 1.0 bar), which is superior to that of most of microporous organic polymers. The facile and cost-effective preparation process and excellent gas sorption properties make these kinds of materials promising candidates for practical applications.

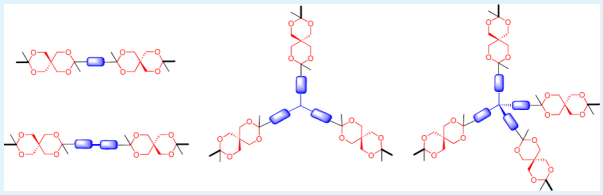

KEYWORDS: *microporous organic polymers, ketal linkage, spiro skeleton, hydrogen storage, carbon dioxide uptake*

INTRODUCTION

Compared with conventional microporous materials[1] (i.e., zeolites and activated carbon) and advanced metal–organic frameworks,[2] the pursuit of novel microporous organic polymers has been rising rapidly in recent years.[3,4] The preparation of microporous organic polymers, containing hyper-cross-linked polymers (HCPs),[5] polymers of intrinsic microporosity (PIMs),[6] conjugated microporous polymers,[7] porous aromatic frameworks (PAFs), and covalent–organic frameworks (COFs),[8] is a great challenge compared with their meso/macroporous counterparts. During removal of the solvents and/or templates from the as-prepared organic porous materials, the much higher surface energies and larger capillary pressures should be overcome. Therefore, in order to preserve the nature of microporosity in the obtained materials, a judicious selection of the monomers and their linkages is needed.[9] In general, the design of rigid, nonplanar, and contorted monomers and highly efficient coupling/condensation chemistries should be empirically considered.[10] The irreversible condensation reactions are usually utilized to construct the polymer chains/branches, which pack so inefficiently in the solid state as to leave much free volume (i.e., microporosity).[11] The polymers of intrinsic microporosity provide an exemplification for the verification of this hypothesis.[9]

To date, a large diversity of synthetic monomers and methodologies to prepare microporous organic polymers have been developed.[12] However, a multistep synthetic route for most monomers is employed, while various heavy/transition-metal catalysts are utilized to catalyze polymerization. All of these complicated processes and precious metal catalysts are prone to limit the wide use of microporous materials in industry.[13] Therefore, our group has been devoted to the preparation of microporous organic polymers using easily obtained or commercially available monomers with a simple and non-metal-catalyzed condensation. For example, aldol self-condensation of aromatic multiacetyl compounds using thionyl chloride as the catalyst,[14] a benzimidazole-forming reaction between bisquinone and multiformyl compounds using no catalyst,[15] and benzoin condensation of multiformyl compounds using *p*-toluenesulfonic acid as the catalyst[16] were utilized to construct microporous polymers. Meanwhile, Schiff base chemistry,[17] a polyimide-forming reaction between melamine and dianhydrides,[18] and a dioxane-forming reaction between catechol and a difluoroaryl unit[6] were also reported.

Recently, Abdel-Razik and El-Bahy reported a kind of "spiroketal" polymer synthesized through 1,3-dioxol-forming polymerization between pentaerythritol and different substituted cyclohexa-1,4-diones.[19] Their polymers can be soluble in many polar solvents, which is similar to the processing polymers of intrinsic microporosity.[10] However, the so-called "spiroketal" is a diketal linkage and not a spiroketal on the basis of the nomenclature. A true spiroketal moiety means that a spiro atom is directly connected at the same time by two oxygen atoms originating from ketone and diol.[20] In the skeletal structure of the obtained polymers, two ketal moieties are connected through a sp^3 carbon atom as a spiro center. It is important for the spiro or contorted atoms to prevent close packing of the polymer matrix, giving an amorphous microporous material.[21] Therefore, the preparation of ketal-linked

Received: January 19, 2013
Accepted: April 29, 2013
Published: April 29, 2013

   dx.doi.org/10.1021/am400251h | ACS Appl. Mater. Interfaces 2013, 5, 4166–4172

polymers might be an essential prototypal condensation, considering that the starting materials (polyol and dione compounds), catalyst (*p*-toluenesulfonic acid), and solvents (benzene or toluene) are all commercially available. In order to expand the practical value of ketal-linked polymers, we synthesized four insoluble ketal-linked porous organic polymers (**KPOPs**) derived from pentaerythritol and different aromatic acetyl-containing compounds. Compared with the results reported by Abdel-Razik and El-Bahy,[19] the obtained polymers possess a higher degree of cross-linking, which results in a higher specific surface area. The highest Brunauer–Emmett–Teller (BET) specific surface area among all polymers is approaching 1000 m^2 g^{-1}. Furthermore, their gas (hydrogen and carbon dioxide) sorption capacities are also investigated. Significantly, the highest hydrogen uptake can reach 1.96 wt % at 77 K and 1.0 bar. The facile and inexpensive preparation process and excellent gas storage properties can make ketal-linked porous organic polymers promising candidates for industrial applications.

EXPERIMENTAL SECTION

Materials and Methods. Acetyl chloride, ferrocene, biphenyl, pentaerythritol, *p*-toluenesulfonic acid, and *o*-dichlorobenzene were purchased from Beijing Chemical Reagent Corp., and ferrocene was purified by sublimation prior to use. Anhydrous aluminum chloride was purchased from Aldrich. Ethyl acetate, petroleum ether, dichloromethane, acetone, and other chemical reagents were used as received. 1,3,5-Triphenylbenzene and tetraphenylmethane were synthesized according to the reported procedures, respectively.[22,23] The detailed synthesis procedures of 1,1′-diacetylferrocene (**M1**), 4,4′-diacetylbiphenyl (**M2**), 1,3,5-tris(4-acetylphenyl)benzene (**M3**), and tetrakis(4-acetylphenyl)methane (**M4**) are included in the Supporting Information. All condensation reactions were operated using the standard Schlenk-line technique.

Preparation of KPOPs. A mixture of **M1** (35.1 mg, 0.13 mmol), pentaerythritol (17.7 mg, 0.13 mmol), and *p*-toluenesulfonic acid was suspended in *o*-dichlorobenzene (4.00 mL). After ultrasonication for 0.5 h, the mixture was degassed by at least three freeze–pump–thaw cycles. The tube was frozen at 77 K (liquid-nitrogen bath) and evacuated to high vacuum and flame-sealed. After 180 °C for 72 h, the reaction mixture gave a solid in quantitative yield. This solid was filtered and washed with water, ethanol, acetone, and dichloromethane, subsequently. The product, denoted as **KPOP-1**, was dried in vacuo at 120 °C for more than 12 h.

Similar to the preparation of **KPOP-1**, **M2** (31.0 mg, 0.13 mmol), **M3** (37.5 mg, 0.087 mmol), or **M4** (31.8 mg, 0.065 mmol) was used to afford **KPOP-2**, **KPOP-3**, or **KPOP-4** in quantitative yield, respectively.

Instrumental Characterization. ^{1}H NMR spectra were recorded on a Bruker DMX400 NMR spectrometer, with tetramethylsilane as an internal reference. Solid-state cross-polarization/magic-angle-spinning (CP/MAS) ^{13}C NMR measurements were performed on a Bruker Avance III 400 spectrometer. Thermogravimetric analysis (TGA) was performed on a Pyris Diamond thermogravimetric/differential thermal analyzer by heating the samples at 10 °C min^{-1} to 800 °C in an atmosphere of nitrogen. IR spectra were recorded in KBr pellets using a Spectrum One Fourier transform infrared (FT-IR) spectrometer (PerkinElmer Instruments Co. Ltd., USA). The IR sample was prepared by dispersing the polymer in KBr and compressing the mixtures to form disks, and 15 scans were signal-averaged. Transmission electron microscopy (TEM) observations were carried out using a Tecnai G^2 F20 U-TWIN microscope (FEI, USA) at an accelerating voltage of 200 kV. The TEM sample was prepared by dropping ethanol suspensions of **KPOP-1**–**KPOP-4** onto a copper grid, respectively. Field-emission scanning electron microscopy (SEM) observations were performed on a Hitachi S-4800 microscope (Hitachi, Ltd., Japan) operating at an accelerating voltage of 6.0 kV. SEM samples were prepared by dropping ethanol suspensions of **KPOP-1**–**KPOP-4** on a silicon wafer and then air drying. Nitrogen adsorption–desorption and hydrogen adsorption experimentations were conducted using an ASAP 2020 M+C surface area and porosity analyzer (Micromeritics, USA). Carbon dioxide uptake experimentation was performed using a TriStar II 3020 accelerated surface area and porosity analyzer (Micromeritics, USA). Before measurement, the samples were degassed in vacuo at 120 °C for more than 12 h. A sample of ca. 100 mg was used for the gas sorption measurements. The gas sorption experiments were performed at least two times. The specific surface area was calculated from nitrogen adsorption data by BET analysis in the relative pressure (P/P_0) range from 0.01 to 0.10 (see the Supporting Information), whereas the pore size and pore-size distribution were estimated through the original density functional theory (DFT). The total pore volume was calculated from nitrogen adsorption–desorption isotherms at P/P_0 = 0.99, whereas the micropore surface area and micropore volume were calculated from nitrogen adsorption–desorption isotherms using the *t*-plot method.

RESULTS AND DISCUSSION

To construct ketal-linked microporous organic polymers, several aromatic diacetyl (**M1** and **M2**), triacetyl (**M3**), and tetraacetyl (**M4**) building blocks (Figure 1) have been

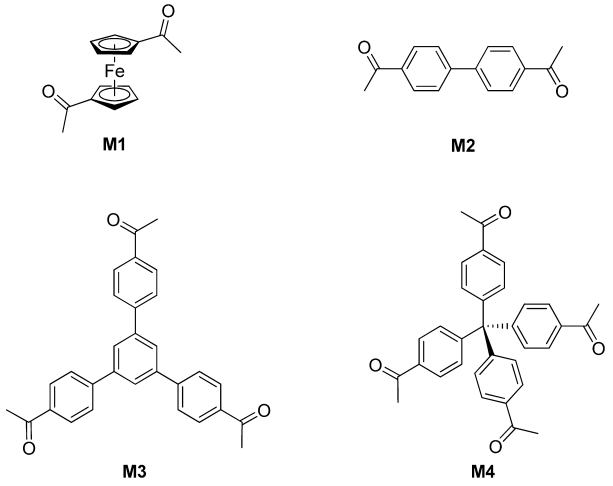

Figure 1. Structures of acetyl-containing building blocks (**M1**–**M4**) used to prepare ketal-linked microporous organic polymers.

synthesized through Friedel–Crafts acylation of corresponding aromatic compounds in high yields. The model reaction between pentaerythritol and acetophenone, which can be catalyzed by protic acid or Lewis acid, to generate a linkage with two ketal moiety connected by a contorted carbon atom is shown in Scheme 1. It is well-known that the ketal moiety is usually utilized as a protective group of ketone.[20] Meanwhile, the aromatic ketal moieties are key substructures in biologically active natural products[24] and pharmaceuticals.[25] Thus, the facile formation of ketal moieties makes it an effective linkage to cross-link nonlinear rigid monomers. By employing the same method as that reported by Abdel-Razik and El-Bahy,[19] we selected a wide range of monomers, including flexible and three-dimensional tetrahedral scaffolds, and obtained a series of insoluble microporous networks with high degrees of cross-linking. Owing to the higher reaction temperature needed, *o*-dichlorobenzene with a boiling point approaching 180 °C is selected as the solvent instead of benzene. A sealed-tube polymerization method is employed to prepare the ketal-linked polymers. Compared with the conventional flask method, the materials obtained from sealed-tube polymerization possess

Scheme 1. Schematic Representation of a Ketal-Forming Reaction

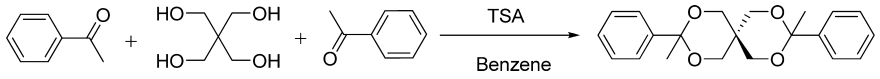

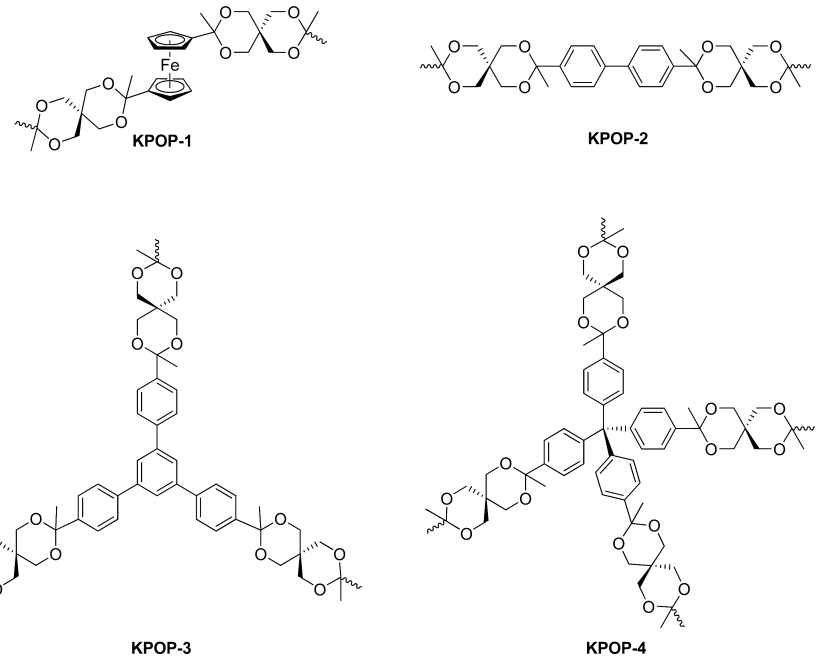

Figure 2. Ideal structures of ketal-linked microporous organic polymers **KPOP-1**–**KPOP-4** by the reaction of pentaerythritol with acetyl-containing building blocks.

excellent performance according to our previous results.[14,15] The closed reaction system and anhydrous oxygen-free conditions show a positive impact on the degree of polymerization and the porosity of the obtained polymers. The aromatic acetyl monomers and pentaerythritol were suspended in *o*-dichlorobenzene, and *p*-toluenesulfonic acid as the catalyst was also added into the reaction system. After polymerization in a sealed tube at 180 °C for 72 h, four polymers (**KPOP-1**–**KPOP-4**) were formed in quantitative yield. For comparison, we also performed this polymerization by employing the conventional flask method, which provides open atmospheric reaction conditions. The gas uptake performance of the resulting polymers is rather poor, and the BET specific surface area is lower than 100 $m^2\ g^{-1}$. Compared to the conventional flask method, the sealed-tube method provides closed, anhydrous, and oxygen-free conditions. A closed reactor can be allowed to treat a higher reaction temperature. The absence of water and oxygen could cause the reaction to occur more thoroughly. Thus, a higher degree of condensation products might be obtained compared with the conventional flask method. The ideal structures of these ketal-linked microporous organic polymers are shown in Figure 2. The two cyclic diketals can be formed by the reaction of pentaerythritol with two different acetyls. Moreover, the hydroxyl groups of pentaerythritol molecules can react with four different acetyls at most, and branched hemiketal linkages are formed (Figure S1, Supporting Information). These two kinds of situations might coexist in the preparation process. This ideal linear structure with a certain cross-linking for **KPOP-1** and **KPOP-2** is different from that of linear PIMs, which can be soluble in polar organic solvents. All of the obtained polymers **KPOPs** are stable and insoluble in common organic solvents such as dichloromethane, ethanol, acetone, and *N*,*N*-dimethylformamide, indicative of a high degree of cross-linking.

The thermal stability of the obtained materials was investigated by TGA (Figure S2, Supporting Information). The thermal decomposition temperature of these polymers is up to 200 °C. The weight loss below 120 °C is generally attributed to evaporation of adsorbed water or trapped gas molecules in the micropores. With an increase in the temperature, all of the polymers show a continuous mass percentage loss and the residual mass is in the range of 60–70 wt %. As seen from the TGA traces, the polymer **KPOP-3** shows the highest thermal stability among these four polymers and exhibits the highest degree of ketal formation with triphenylbenzene as the core. The stability of the obtained polymers against acidic and basic hydrolysis is also investigated, where the polymer **KPOP-4** is selected as an example. The polymer was suspended in the acidic (HCl, 1.0 mol L^{-1}) or basic (NaOH, 1.0 mol L^{-1}) aqueous solution and stirred for 5 days. The calculated BET specific surface area merely increases by 60 $m^2\ g^{-1}$ after acid treatment, which is in the range of instrumental systematic error. However, the BET specific surface area reduces remarkably after base treatment (Figure S10, Supporting Information), indicating that a significant amount of basic hydrolysis took place. Thus, the polymers **KPOPs** demonstrate an acid-resistant and basic-hydrolyzable character.

The structures of prepared ketal-linked polymers were confirmed by FT-IR spectroscopy. In all spectra of the four polymers, bands that can be attributed to the carbonyl stretching of acetyl monomers at 1680–1690 cm^{-1} and the hydroxyl stretching of pentaerythritol at 3337 cm^{-1} are significantly reduced (Figures S3–S6, Supporting Information),

dx.doi.org/10.1021/am400251h | *ACS Appl. Mater. Interfaces* 2013, 5, 4166–4172

indicating that an expected cross-linking takes place between acetyl monomers and pentaerythritol. Significantly, absorption peaks at 1706−1720 cm^{-1} assigned to the stretching vibration of the six-membered ring of the ketal moiety with one carbon atom connected at the same time by two oxygen atoms $[-C(O)_2-]$ indicate that the desired polymers have been synthesized successfully. The characteristic aliphatic C−H and C−O stretching vibration bands at ca. 2900 and 1100 cm^{-1} are also observed in the resultant polymers. The signals of the fingerprint region are preserved, indicating that the aromatic structures of monomers get into the skeletons of the obtained polymers.

All of the obtained polymers were characterized by solid-state CP/MAS ^{13}C NMR spectroscopy. The assignment of the resonances in the ^{13}C NMR spectra of the ketal-linked polymers is shown in Figures 3 and S7 (Supporting Information). For **KPOP-3**, there are two major peaks at approximately 141 and 128 ppm and three faint peaks at ca. 78, 52, and 19 ppm, respectively (Figure 3). The two major resonances at 141 and 128 ppm can be assigned to the carbon of aromatic substituted and unsubstituted atoms. The low-intensity peak at 78 ppm is observed in the obtained polymers, which corresponds to the carbon atom connected by the oxygen atoms in the ketal moieties. The resonance at 19 ppm is ascribed to the methyl group originating from the acetyl monomers, whereas the resonance at 52 ppm can be ascribed to the quaternary carbon atoms originating from pentaerythritol. However, the spectrum of **KPOP-4** shows a different resonance at 65 ppm, which can be assigned to quaternary carbon atoms originating from the tetraphenylmethane monomer (Figure S7, Supporting Information). The resonance for the carbon atom in the alkoxyl groups might overlap with that of the quaternary carbon.[26] In general, the FT-IR and solid-state ^{13}C NMR data support our proposed structures.

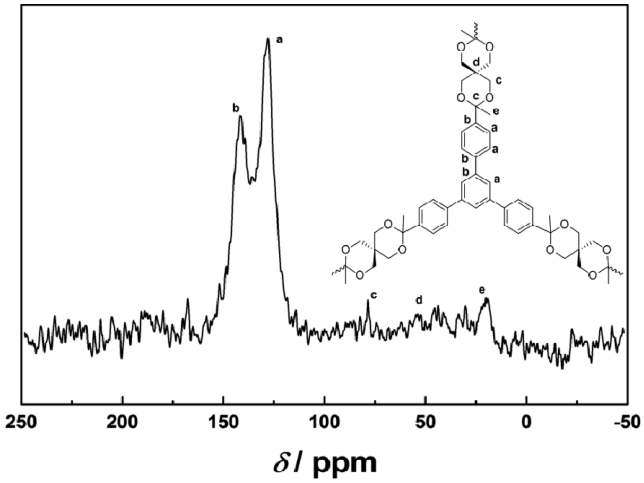

Figure 3. Solid-state CP/MAS ^{13}C NMR spectra of **KPOP-3** recorded at a MAS rate of 5 kHz.

The morphology of the ketal-linked polymers was investigated by SEM. The SEM images reveal regular microspheres of 2 μm for **KPOP-2**, whereas no obvious morphology for **KPOP-1**, **KPOP-3**, and **KPOP-4** (Figures 4 and S8, Supporting Information). These polymers exhibit an amorphous nature and consist of irregular nanoparticles and nanoplatelets. The high-resolution TEM (HR-TEM) images confirm that they possess a disordered structure (Figure 3c,d).

Nitrogen adsorption−desorption isotherm measurements can analyze the porous properties of microporous networks. Figure 5a shows the nitrogen adsorption and desorption isotherms for the obtained ketal-linked microporous organic polymers. The polymeric networks of **KPOP-1**, **KPOP-2**, and **KPOP-4** give rise to type I nitrogen gas sorption isotherm according to the IUPAC classification.[27] The isotherms show a high gas uptake at a relative pressure (P/P_0) less than 0.02, a flat course at the middle and high relative pressures, indicating a significant microporosity nature in the resulting polymers.

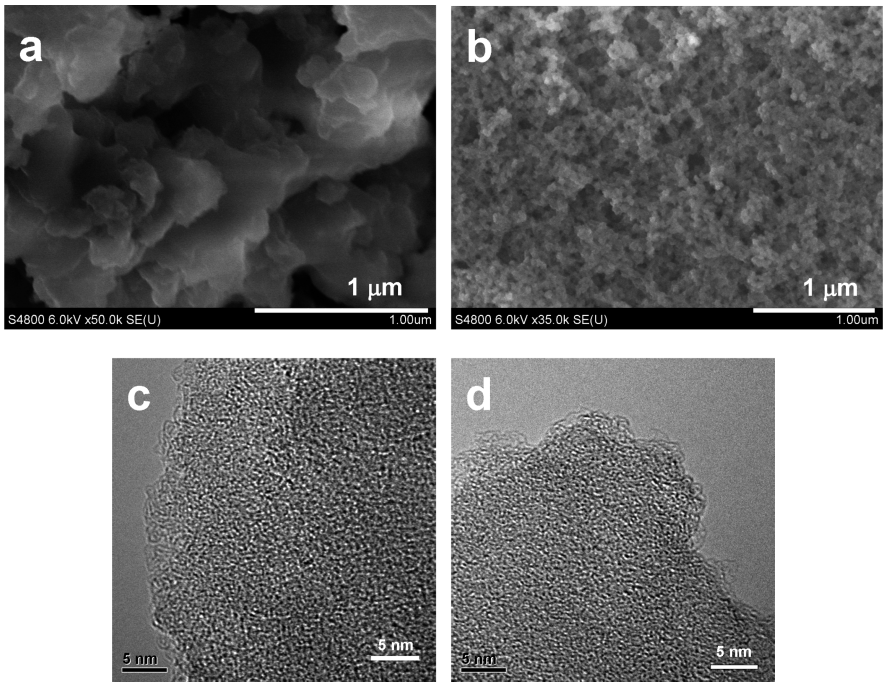

Figure 4. SEM (a and b) and HR-TEM (c and d) images of **KPOP-1** (a and c), **KPOP-3** (b), and **KPOP-4** (d).

dx.doi.org/10.1021/am400251h | ACS Appl. Mater. Interfaces 2013, 5, 4166−4172

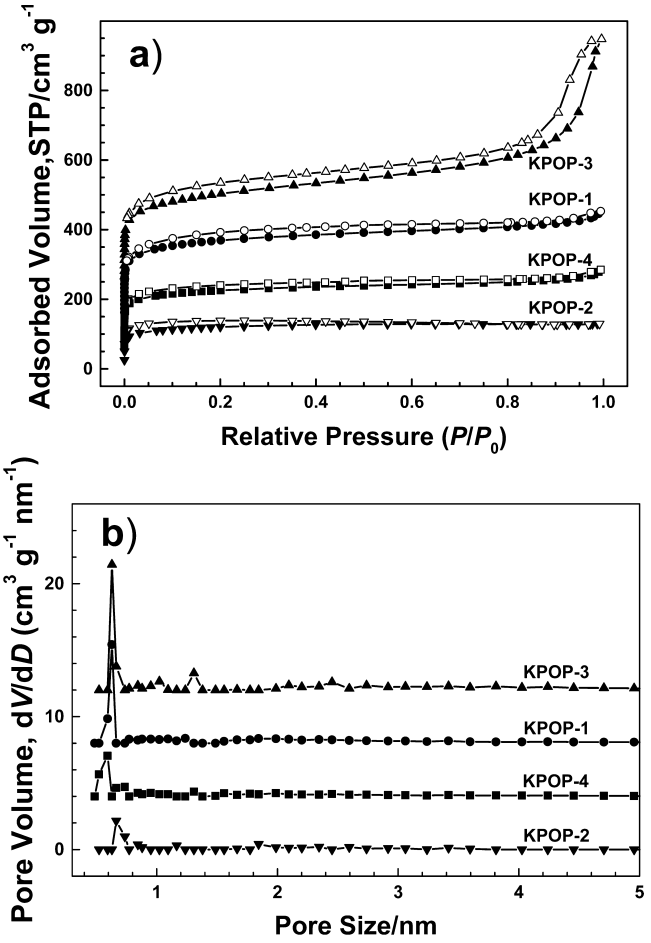

Figure 5. (a) Nitrogen adsorption−desorption isotherms of **KPOP-1** (circle), **KPOP-2** (down triangle), **KPOP-3** (up triangle), and **KPOP-4** (square) at 77 K. The isotherms of **KPOP-4**, **KPOP-1**, and **KPOP-3** have been offset by 100 units for the purpose of clarity. (b) Pore-size distribution profiles calculated by the original DFT method. The profiles of **KPOP-4**, **KPOP-1**, and **KPOP-3** have also been offset by 2 units for the purpose of clarity.

However, the isotherm for **KPOP-3** exhibits a combination of type I and II nitrogen sorption isotherm, in which there is a continuous uptake at high relative pressure. This phenomenon can be interpreted as interparticulate voids arising from loose packing of some nanoparticles.[28] A small hysteresis can be observed for all of the isotherms, which is normal for the amorphous microporous organic polymers.[29] Listed in Table 1 are the key porosity properties derived from the isotherms, such as the BET specific surface area, micropore surface area, micropore volume, total pore volume, and pore size. The specific surface area is calculated by the BET method using different pressure ranges[30] (Figure S9 and Table S1, Supporting Information). The highest BET specific surface area up to 950 $m^2\ g^{-1}$ was obtained for the polymer **KPOP-3** with a total pore volume of 1.08 $cm^3\ g^{-1}$ determined at P/P_0 = 0.99. Figure 5b shows the pore-size distribution profiles of the four microporous polymers, as calculated using the original DFT. In the micropore region, only one steep peak is observed, which is located at ca. 0.64, 0.67, 0.63, and 0.58 nm for the four porous polymers, respectively.

The hydrogen and carbon dioxide adsorption properties of the polymers were also investigated by volumetric methods (Figure 6 and Table 1). Hydrogen storage capacities for these

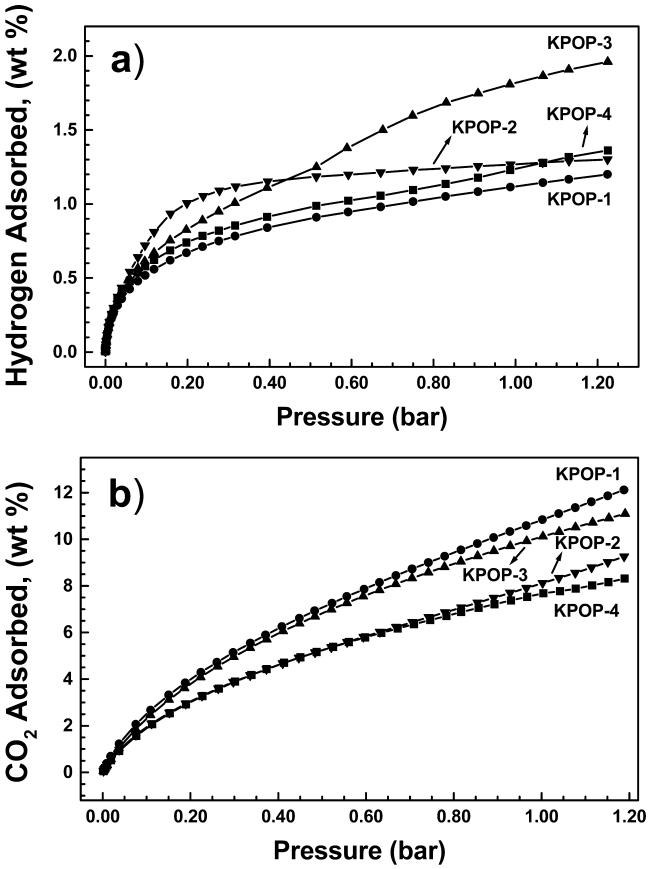

Figure 6. Gravimetric hydrogen (a) and carbon dioxide (b) adsorption isotherms for **KPOP-1** (circles), **KPOP-2** (down triangles), **KPOP-3** (up triangles), and **KPOP-4** (squares) at 77 and 273 K, respectively.

polymers vary between 1.20 and 1.96 wt % measured at 77 K and 1.0 bar. Obviously, the polymer **KPOP-4** exhibits a

Table 1. Porosity Properties and Gas Adsorption Capacities of Microporous Polymers KPOP-1−KPOP-4

polymer	S_{BET} ($m^2\ g^{-1}$)[a]	S_{micro} ($m^2\ g^{-1}$)[b]	V_{micro} ($cm^3\ g^{-1}$)[c]	V_{total} ($cm^3\ g^{-1}$)[d]	D_{pore} (nm)[e]	H_2 uptake (wt %)[f]	CO_2 uptake (wt %)[g]
KPOP-1	810	420	0.19	0.50	0.64	1.20	12.1
KPOP-2	520	260	0.12	0.27	0.67	1.30	9.26
KPOP-3	950	390	0.18	1.08	0.63	1.96	11.1
KPOP-4	660	390	0.18	0.36	0.58	1.36	8.31

[a]Specific surface area calculated from the nitrogen adsorption isotherm using the BET method in the relative pressure (P/P_0) range from 0.01 to 0.10. [b]Micropore surface area calculated from the nitrogen adsorption isotherm using the *t*-plot method. [c]Micropore volume calculated from the nitrogen adsorption isotherm using the *t*-plot method. [d]Total pore volume at P/P_0 = 0.99. [e]Pore size calculated from the nitrogen adsorption isotherm using the DFT method. [f]Hydrogen gravimetric uptake capacities at 1.0 bar and 77 K. [g]Carbon dioxide gravimetric uptake capacities at 1.0 bar and 273 K.

dx.doi.org/10.1021/am400251h | ACS Appl. Mater. Interfaces 2013, 5, 4166−4172

hydrogen uptake (1.36 wt %) similar to the polymers **KPOP-1** (1.20 wt %) and **KPOP-2** (1.30 wt %), whereas the polymer **KPOP-3** possesses the highest hydrogen storage capacity up to 1.96 wt %. The adsorption and desorption branches of the hydrogen sorption isotherm for the polymer **KPOP-3** are almost fully reversible (Figure S11, Supporting Information). These values are superior to those of the triptycene-based PIMs (0.74−1.83 wt %), HCPs (0.80−1.70 wt %), and COFs/PAFs (0.90−1.50 wt %),[31] while they are inferior to those of a spiro(fluorine-9,9′-xanthene)-based copolymer (SPOP-3, 2.22 wt %)[32] and microporous polycarbazole materials (CPOP-1, 2.80 wt %).[33] The narrow pore size of around 0.60 nm and large total pore volume in the resulting polymers might be responsible for this excellent hydrogen uptake.[34,35] The adsorption isotherms for the polymers **KPOP-3** and **KPOP-1** show moderate capacities of carbon dioxide up to 11.1 wt % (56 cm^3 g^{-1}, STP) and 12.1 wt % (62 cm^3 g^{-1}, STP), respectively. The polar linkage in the ketal-linked polymers might have a rather high affinity toward carbon dioxide through local-dipole/quadrupole interactions.[36]

CONCLUSIONS

In summary, we have presented a facile approach to preparing insoluble ketal-linked microporous organic polymers through condensation between pentaerythritol and different aromatic acetyl-containing monomers. Both of the starting materials, catalysts, and solvents are all commercially available industrial raw materials. In addition, no heavy metal is involved in the whole process. The FT-IR and solid-state CP/MAS ^{13}C NMR spectroscopy confirmed the occurrence of ketal linkages in the resulting polymers. For polymers obtained by the sealed-tube method, the polymer **KPOP-3** possesses the highest BET specific surface area up to 950 m^2 g^{-1}. A nice hydrogen storage (1.96 wt %, at 77 K and 1.0 bar) and moderate carbon dioxide capacity (11.1 wt %, at 273 K and 1.0 bar) for **KPOP-3** are also demonstrated. When the cost-effective preparation process (i.e., inexpensive starting compounds and metal-free catalysts) and the resulted excellent gas sorption properties are combined, the ketal-linked microporous organic polymers could be a new kind of high-performance network in materials science.

ASSOCIATED CONTENT

Supporting Information

Details of the syntheses of monomers, TGA data, FT-IR data, solid-state CP/MAS ^{13}C NMR spectra, SEM images, and BET surface area data. This material is available free of charge via the Internet at http://pubs.acs.org.

AUTHOR INFORMATION

Corresponding Author

*Fax: +86 10 8254 5576. E-mail: hanbh@nanoctr.cn.

Notes

The authors declare no competing financial interest.

ACKNOWLEDGMENTS

Financial support of the National Science Foundation of China (Grants 91023001 and 60911130231), the Ministry of Science and Technology of China (National Major Scientific Research Program; Grant 2011CB932500), and the Chinese Academy of Sciences (Knowledge Innovation Program; Grant KJCX2-YW-H21) is acknowledged.

REFERENCES

(1) Mangun, C. L.; Yue, Z.; Economy, J. *Chem. Mater.* **2001**, *13*, 2356−2360.
(2) Eddaoudi, M.; Kim, J.; Rosi, N.; Vodak, D.; Wachter, J.; Yaghi, O. M. *Science* **2002**, *295*, 469−453.
(3) Wu, D.; Xu, F.; Sun, B.; Fu, R.; He, H.; Matyjaszewski, K. *Chem. Rev.* **2012**, *112*, 3959−4015.
(4) Thomas, A. *Angew. Chem., Int. Ed.* **2010**, *49*, 8328−8344.
(5) Tsyurupa, M. P.; Davankov, V. A. *React. Funct. Polym.* **2002**, *53*, 193−203.
(6) Budd, P. M.; Ghanem, B. S.; Makhseed, S.; Mckeown, N. B.; Msayib, K. J.; Tattershall, C. E. *Chem. Commun.* **2004**, *40*, 230−231.
(7) Jiang, J.-X.; Su, F.; Trewin, A.; Wood, C. D.; Cooper, A. I. *Angew. Chem., Int. Ed.* **2007**, *46*, 8574−8578.
(8) Katsoulidis, A. P.; Kanatzidis, M. G. *Chem. Mater.* **2011**, *23*, 1818−1824.
(9) McKeown, N. B.; Budd, P. M. *Macromolecules* **2010**, *43*, 5163−5176.
(10) McKeown, N. B.; Budd, P. M.; Msayib, K. J.; Ghanem, B. S.; Kingston, H. J.; Tattershall, C. E.; Makhseed, S.; Reynolds, K. J.; Fritsch, D. *Chem.—Eur. J.* **2005**, *11*, 2610−2620.
(11) Mckeown, N. B.; Budd, P. M.; Book, D. *Macromol. Rapid Commun.* **2007**, *28*, 995−1002.
(12) Dawson, R.; Cooper, A. I.; Adams, D. J. *Prog. Polym. Sci.* **2012**, *37*, 530−563.
(13) Viela, F.; Zhang, K.; Antonietti, M. *Energy Environ. Sci.* **2012**, *5*, 7819−7832.
(14) Zhao, Y.-C.; Zhou, D.; Chen, Q.; Zhang, X.-J.; Bian, N.; Qi, A.-D.; Han, B.-H. *Macromolecules* **2011**, *44*, 6382−6388.
(15) Zhao, Y.-C.; Cheng, Q.-Y.; Zhou, D.; Wang, T.; Han, B.-H. *J. Mater. Chem.* **2012**, *22*, 11509−11514.
(16) Zhao, Y.-C.; Wang, T.; Zhang, L.-M.; Cui, Y.; Han, B.-H. *ACS Appl. Mater. Interfaces* **2012**, *4*, 6975−6981.
(17) Schwab, M. G.; Fassbender, B.; Spiess, H. W.; Thomas, A.; Feng, X.; Müllen, K. *J. Am. Chem. Soc.* **2009**, *131*, 7216−7217.
(18) Luo, Y.; Li, B.; Liang, L.; Tan, B. *Chem. Commun.* **2011**, *47*, 7704−7706.
(19) Abdel-Razik, H. H.; El-Bahy, Z. M. *Chin. J. Polym. Sci.* **2011**, *29*, 450−455.
(20) Wang, X.; Han, Z.; Wang, Z.; Ding, K. *Angew. Chem., Int. Ed.* **2012**, *51*, 936−940.
(21) Maly, K. E. *J. Mater. Chem.* **2009**, *19*, 1781−1787.
(22) Elmorsy, S. S.; Pelter, A.; Smith, K. *Tetrahedron Lett.* **1991**, *32*, 4175−4176.
(23) Tanemura, K.; Suzuki, T.; Nishida, Y.; Horaguchi, T. *Tetrahedron Lett.* **2008**, *49*, 6419−6422.
(24) Brasholz, M.; Sörgel, S.; Azap, C.; Reißig, H.-U. *Eur. J. Org. Chem.* **2007**, *2007*, 3801−3814.
(25) Hu, Y.-C.; Wu, X.-F.; Gao, S.; Yu, S.-S.; Liu, Y.; Qu, J.; Liu, J.; Liu, Y.-B. *Org. Lett.* **2006**, *8*, 2269−2272.
(26) Garibay, S. J.; Weston, M. H.; Mondloch, J. E.; Colón, Y. J.; Farha, O. K.; Hupp, J. T.; Nguyen, S. T. *CrystEngComm* **2013**, *15*, 1515−1519.
(27) Sing, K. S. W.; Everett, D. H.; Haul, R. A. W.; Moscou, L.; Pierotti, R. A.; Rouquérol, J.; Siemieniewska, T. *Pure Appl. Chem.* **1985**, *57*, 603−619.
(28) Yu, H.; Shen, C.; Tian, M.; Qu, J.; Wang, Z. *Macromolecules* **2012**, *45*, 5140−5150.
(29) Weber, J.; Schmidt, J.; Thomas, A.; Böhlmann, W. *Langmuir* **2010**, *26*, 15650−15656.
(30) Dawson, R.; Laybourn, A.; Clowes, R.; Khimyak, Y. Z.; Adams, D. J.; Cooper, A. I. *Macromolecules* **2009**, *42*, 8809−8816.
(31) Ghanem, B. S.; Hashem, M.; Harris, K. D. M.; Msayib, K. J.; Xu, M.; Budd, P. M.; Chaukura, N.; Book, D.; Tedds, S.; Walton, A.; McKeown, N. B. *Macromolecules* **2010**, *43*, 5287−5294.
(32) Chen, Q.; Wang, J.-X.; Wang, Q.; Bian, N.; Li, Z.-H.; Yan, C.-G.; Han, B.-H. *Macromolecules* **2012**, *44*, 7987−7993.

(33) Chen, Q.; Luo, M.; Hammershøj, P.; Zhou, D.; Han, Y.; Laursen, B. W.; Yan, C.-G.; Han, B.-H. *J. Am. Chem. Soc.* **2012**, *134*, 6084−6087.
(34) Han, S. S.; Mendoza-Cortés, J. L.; Goddard, W. A. *Chem. Soc. Rev.* **2009**, *38*, 1460−1476.
(35) Germain, J.; Fréchet, J. M. J.; Svec, F. *Small* **2009**, *5*, 1098−1111.
(36) Rabbani, M. G.; El-Kaderi, H. M. *Chem. Mater.* **2011**, *23*, 1650−1653.